Optimal Design of Electrically-Small Loop Receiving Antenna

Timothy Bolton[1], * and Morris B. Cohen[2]

Abstract—There is a large body of literature for electrically-small loop receiving antennas including more recent work in demagnetization effects for magnetic materials which are used for reducing antenna size. Optimal design of loop antennas requires understanding the electromagnetic principles and is limited by the accuracy of predicting the electromagnetic parameters (resistance, inductance, capacitance, effective permeability, sensitivity). We present the design principles for electrically-small loop receiving antennas including recommended formulas, a novel approach to optimal design and an application example for use in the VLF/LF band (1–100 kHz) for two different ferrite-core loop antennas including the optimum coil parameters. Using a ferrite magnetic core greatly complicates analysis and prediction of resistance, inductance, and sensitivity as a function of frequency due to the dependence on core material properties, core geometry, and wire coil geometry upon the core (capacitance is typically negligibly affected). Experimental results for the two ferrite-core loop antennas and an air-core loop antenna validate the optimal design approach with good overall agreement to theoretical prediction of resistance, inductance, and sensitivity. Discussion and comparison between air-core and ferrite-core designs demonstrate the trade-off between outer diameter, length, and mass vs. sensitivity.

1. INTRODUCTION

Electrically-small loop (ESL) receiving antennas find use in a variety of fields such as communications and geophysics. Since the ESL can be treated as a magnetic dipole, it has the classic figure-eight far-field radiation pattern and can be less sensitive than other antenna types to electric fields, the latter being a common cause of ambient noise. Like electric monopoles and dipoles, the ESL can be loaded with a material to enhance its reception sensitivity — typically a magnetic core made of ferrite. Unlike simple electric monopoles and dipoles, the ESL's sensitivity can be further increased by using multiple coil turns with small change in antenna size.

The various design principles involved in ESLs can be found in most general antenna handbooks. Design specific to magnetic-core ESLs is limited in literature, with [1] being the most comprehensive followed by [2, 3]. In many texts, it is common to greatly simplify core shape and coil geometry effects (textbooks such as [4]) due to the complexity and difficulty in theoretical analysis.

While loops have been analyzed for over 150 years — such as Maxwell's *Treatise on electricity and magnetism* (1873) — there continue to be advances in theory and analysis. In particular, the topic of demagnetization has received significant attention in recent decades such as by Chen et al. [5], as it causes the magnetic field to be substantially less in practice than the material permeability property would suggest. Despite advances in demagnetization, it is still common to see plots of apparent permeability based on a family of curves based on research in the 1930s and 1940s such as [6]. An exhaustive list of references for analytical and numerical calculations of ESL properties were studied in [1] and compared to measurements.

In this paper, we present in more detail the various design principles as well as a methodology for optimized ESL design, then provide an example including predictions and measured results. The design example is for use with a receiver known as the Atmospheric Weather Electromagnetic System for Observation, Modeling, and Education (AWESOME) receiver which is used for sensitive reception of broadband radio signals (natural and man-made) below 500 kHz. The initial version of the AWESOME is described by [7], and it has been subsequently upgraded to extend the frequency range to ~ 500 kHz and improve the sensitivity by 10–20 dB, amongst other improvements. We limit our design and analysis to 100 kHz signals and below, a band which contains natural radio signals from lightning as well as long-range naval communications, timing and navigation beacons.

2. ESL CIRCUIT MODEL AND PARAMETERS

2.1. ESL Circuit Model

The ESL is effectively a low-frequency, lumped-element inductor and can be accurately modeled as such with a series resistance R and inductance L in parallel with a capacitance C (see Figure 1). These parameters together determine the self-resonant frequency (SRF) of the circuit (in addition to the SRF for coil length and for core length). The voltage generated upon the ESL from an incident field is proportional to the antenna's effective height (which can be related to sensitivity or antenna gain). Additional circuit components may consist of wire leads, transmission lines, and matching circuitry; these should be modeled appropriately.
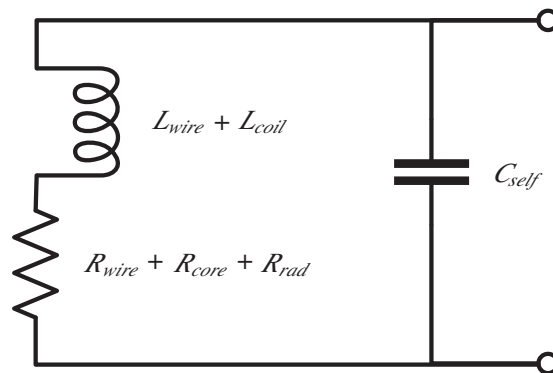
Figure 1. Circuit model of electrically-small loop.

The lumped-element parameters are straightforward to calculate for an air-core ESL [7, 8], but are more difficult for magnetic-core ESLs. This is because the series resistance and inductance depend on the magnetic core's effective permeability, whereas the self-capacitance does not. Self-capacitance does, however, depend on the conductivity of the core (if any) and nearby conductors like a surrounding shield (which can be useful for further decreasing the ESL's sensitivity to electric fields); resistance and inductance are also affected by such. These parameters will be further reviewed in the following sections, though there is extensive literature for each of these.

2.2. Resistance

The equivalent circuit's series resistance R is accurately estimated as a summation of all resistive effects; it is sometimes referred to as the "equivalent series resistance". Typical losses arise from the wire conductor due to skin and proximity effects; from a magnetic core due to hysteresis, eddy current, and Barkhausen effects; and from radiation resistance plus effects from nearby conducting media. These are all frequency dependent.

Wire conductor resistance R_{wire} is equal to the DC resistance R_{dc} multiplied by skin and proximity

effect factors $F_{R,skin}$ and $F_{R,prox}$ (respectively):

$$R_{dc} = \frac{l_{wire}}{\sigma_{cond}A_{cond}}$$

$$R_{wire} = R_{dc}\left(F_{R,skin} + F_{R,prox}\right) \tag{1}$$

where l_{wire} is the length of the wire conductor; σ_{cond} is the conductivity of the conductor; and A_{cond} is the cross-sectional area of the conductor.

Skin effect for a round-wire is well known:

$$F_{R,skin} = \frac{q}{2}\left[\frac{ber\,(q)\,bei'\,(q) - bei\,(q)\,ber'\,(q)}{\left(ber'\,(q)\right)^2 + \left(bei'\,(q)\right)^2}\right], \quad q = \frac{r_{cond}\sqrt{2}}{\delta_{cond}}$$

where $ber()$ and $bei()$ are zero-order Kelvin functions (and their derivatives $ber'()$, $bei'()$); r_{cond} is the conductor's radius; and δ_{cond} is the conductor's skin depth.

Proximity effect between round wires (neglecting effects from other nearby conducting media) is analytically rigorous [9] and is typically approximated, estimated by software, or neglected. A useful approximation by equation is found in Knight's frequency-extension of Medhurst's work [10, D. W. Knight, ⟨http://g3ynh.info/zdocs/magnetics/⟩] for a single-layer air-core or Dowell's method for a multi-layer magnetic-core [11, 12]; though the latter has been found to have errors upwards of 60%, it is still often better than other approximations [11, 13]. On a magnetic core, coil turns nearest air-gaps (such as the ends of a rod core) experience the highest proximity effects [11, 14, 15]; this can be minimized by changing the coil shape to a trapezoidal geometry [14].

Instead of round insulated wire, Litz wire may be used to minimize conductor losses at low frequencies. Design equations are listed and compared in the literature ([12, 16–20], and especially [15]). While Litz can reduce the skin and proximity effect losses, the wire is more expensive and has a decreased window utilization (conductor-to-insulator radio).

Magnetic core losses are sometimes approximated by multiplying the inductive reactance by the magnetic core's measured loss tangent $\tan(\delta_m)$. However, measurements [1, 2] indicate that a correction factor is required to account for the geometry-dependent flux distribution [1]:

$$R_{core} \approx \omega L_{coil} \tan\left(\delta_m\right)\left(\frac{\mu_{a,f}}{\mu_i}\right), \quad \tan\left(\delta_m\right) = \frac{\mu_r''}{\mu_i}$$

where ω is the angular frequency; L_{coil} is the coil external inductance (discussed later); and $\mu_{a,f}$, μ_i, and μ_r'', are the core's apparent fluxmetric permeability, initial (relative real) permeability, and relative imaginary permeability, respectively. Core losses can be minimized by choosing a magnetic core material with very low loss tangent (low conductivity) and/or separating the core into insulated laminations to reduce eddy losses.

The radiation resistance R_{rad} of an ESL in free-space is well known (it is difficult to analytically derive otherwise) [2]:

$$R_{rad} = \frac{\eta_{ins}}{6\pi}\beta_{ins}^4\left(\mu_{ext}nA_{coil}\right)^2$$

where η_{ins} and β_{ins} are the characteristic impedance and phase constant of the insulation (assumed non-conducting), respectively; μ_{ext} is the effective external permeability of the magnetic core (discussed later); n is the number of coil turns; and A_{coil} is the area enclosed by the coil.

The resistive influence of nearby media is difficult to solve for but a variety of cases have been analyzed such as an insulated ESL immersed in a conducting medium [21]. Analytical expressions should be corrected for the permeability of the ESL's magnetic core (if any) as in [1].

2.3. Inductance

Just as for the equivalent circuit's series resistance, the series inductance is accurately estimated as a summation of all inductive effects. The wire conductor, coil geometry, magnetic core, and nearby conducting media all contribute to the inductance.

Inductance due to a current flowing through a straight wire conductor is sometimes referred to as conductor internal inductance. Conductor internal inductance L_{wire} is equal to the DC inductance L_{dc} multiplied by skin and proximity effect factors $F_{L,skin}$ and $F_{L,prox}$ (respectively) [1]:

$$L_{dc} = \frac{\mu_0 \mu_{cond} l_{wire}}{8\pi}$$

$$L_{wire} = L_{dc}\left(F_{L,skin} + F_{L,prox}\right)$$

where μ_0 is the absolute permeability of free-space and μ_{cond} is the relative permeability of the conductor.

Conductor resistance and inductance are inversely related [1]:

$$F_{L,skin} = 1/F_{R,skin}, \quad F_{L,prox} = -F_{R,prox}/\left(F_{R,prox} + 1\right)$$

Once a wire is bent, it gains additional inductance sometimes referred to as external inductance; note that in some literature, internal and external inductance are not separated. There is a plethora of literature on different coil geometries' inductance, ranging from analytical derivations to empirical fits (see [1] for a comprehensive list). Often, coils are categorized as either zero-length "rings" (of varying cross-sectional shape) or as solenoidal coils of finite length (for which the ring is the special case of zero length); they may consist of multiple coil turns ("multi-turn") and multiple coil layers ("multi-layer").

Figure 2 compares the inductance (normalized for permeability, coil area, and turn number) of various geometries and equations for rings and solenoids as a function of coil length divided by coil area; they are treated as theoretically ideal and air-core, single-layer. Note that some equations have limited scope but were still included for comparison. For rings and short coils (relative to coil area), a coil of square cross-section has higher inductance followed by circle, isosceles triangle, then equilateral triangle. For long coils (coil length $\gg$ coil area/10), the inductance is dependent on coil area independent of shape; this conclusion matches literature [22].
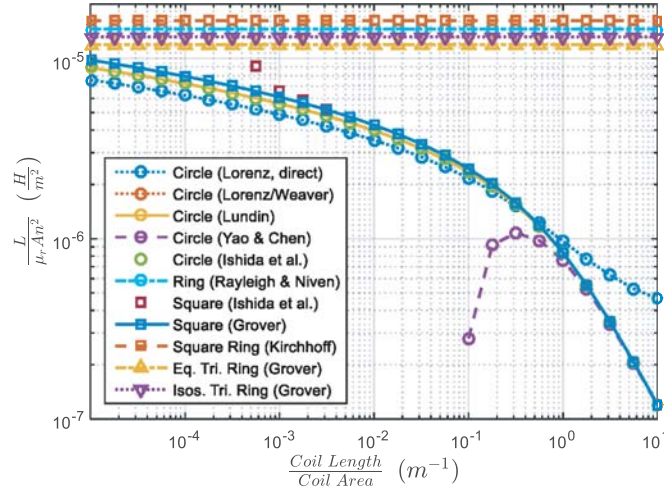
Figure 2. Comparison of air-core inductance formulas for solenoids and rings.

Accurate analytical calculation of an air-core coil's external inductance L_{coil} is typically performed using the well-known current-sheet approximation and a correction for real wire — such as Rosa's and Snow's methods [23–25]. Computational round-off errors can be a problem in the analytical solution, for which some literature attempts to overcome [26–30]. One useful technique is Weaver's adaptation of Snow's method for single-layer (or thin multi-layer) coils. To correct for the effects of a magnetic core, the coil inductance is then multiplied by the core's effective internal permeability μ_{int} (discussed later).

Often, the current-sheet approximation has very high accuracy without correction when the winding pitch (distance between coil turns) is less than coil thickness (wire diameter if single-layer), and the latter is relatively thin compared to the solenoid dimensions. In such cases, Wheeler's famous handbook formula is very accurate for coil length greater than 0.4 times the coil diameter [31]:

$$L_{coil} \approx \frac{0.4\pi^2 \mu_0 \mu_{int} r_{coil}^2 n^2}{l_{coil} + 0.9 r_{coil}}$$

where r_{coil} is the coil radius and l_{coil} is the coil length.

Surrounding conducting media affects the inductance, just as it does the resistance (see above). Shielding the coil can significantly decrease the inductance [32, 33]. Nearby coils' mutual flux linkage should also be considered, although orthogonal coils can typically be ignored. For a more comprehensive treatment and list of literature, see [1].

2.4. Capacitance

The equivalent circuit's self-capacitance C_{self} (also referred to as stray, distributed, or parasitic) is a combination of all capacitive effects. The coil geometry, core, and nearby conductive media (such as a shield) all contribute to the self-capacitance. The self-capacitance is separate from any external capacitor added to resonate the ESL at a frequency.

To wit, there is no accurate, generalized (pseudo-)analytical solution for the self-capacitance of a coil but it is an on-going topic [34–36]. For a single-layer coil in free-space, but connected to a circuit, a self-capacitance arises due to the stored axial electric field of a wave propagating along a helical wire [37] and inter-turn capacitance from separated charges of differing potential due to nonzero resistance along the wire [12]. Separate coil layers also affect the self-capacitance.

A conducting core and/or shield can significantly affect the self-capacitance. As long as the core is non-conducting (such as ferrite), it typically does not significantly affect the self-capacitance (see also [38]). For multi-layer coils, it is reported that a conducting core or shield likely has little impact (increasing the self-capacitance by less than 20%) [39].

2.5. Permeability

As mentioned above, there are several permeability terms to consider which are simple for an air-core but not for a magnetic-core. These terms have various names in literature and are sometimes erroneously confused as the subject is complex. We will concisely describe them here.

The initial (or specified) permeability μ_i of a magnetic material is the real, relative value of the material's permeability as typically measured from coil inductance on a toroid and is ideally independent of coil and core geometry. Initial permeability also depends on frequency, temperature, and external field strength, although we assume room temperature and a sufficiently-weak magnetic field. The material is assumed here to be uniform, isotropic, and linear.

The apparent permeability μ_a is the real, relative value of the permeability when measured from coil voltage generated from a uniform, external magnetic field for a specific core shape and coordinate direction (axial or radial for a cylinder) for either an infinitely-short coil ($\mu_{a,f}$-"fluxmetric" or "ballistic") or for a coil that fully spans the core ($\mu_{a,m}$-"magnetometric"). Apparent permeability μ_a is directly derived from the initial permeability μ_i of the magnetic material and the demagnetization factor N. The relation is [40]:

$$\mu_a = \frac{\mu_i}{1 + N(\mu_i - 1)}$$

The demagnetization factor N depends on the core geometry, core initial permeability μ_i, and coil geometry upon the core. It relates the net magnetic field inside a magnetic core relative to an external field either at the center of the core (fluxmetric, N_f) or integrated over the whole core length (magnetometric, N_m) due to internal magnetic dipole moments opposing an applied field. The demagnetization factor N is a vector — for a cylinder, there is an axial (N_{axial}) and a radial component (N_{radial}) — where we employ the standard convention that the vectoral components sum to 1. This is illustrated and described in Figure 3.
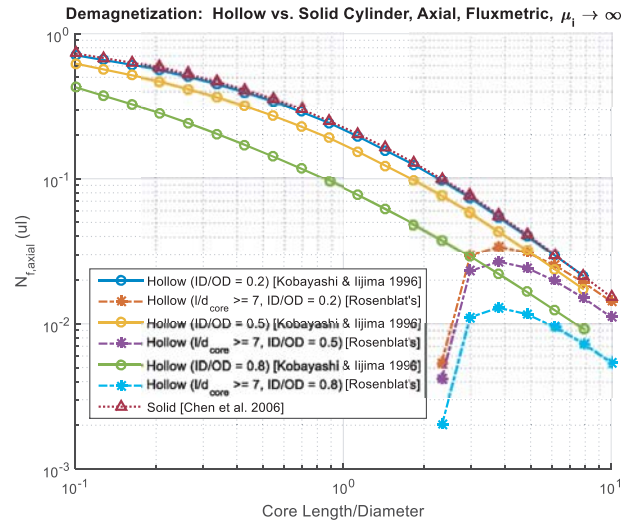
The axial demagnetization factors (fluxmetric and magnetometric) for solid cylinders and spheroids are presented in Figure 4 as a function of length-to-diameter and initial permeability μ_i (using [40]). From Figure 4, the axial demagnetization factors (and apparent permeability) are seen to be approximately the same for very small core length: diameter ratios, but diverge as the ratio approaches 1 and become increasingly dependent on μ_i and coil geometry. Although we focus on circular cylinders here, the demagnetization factor for other shapes are also available (see [1] for an exhaustive list); further, square rods are effectively the same as circular cylinders of equivalent cross-sectional area (within 3.5% [41]).
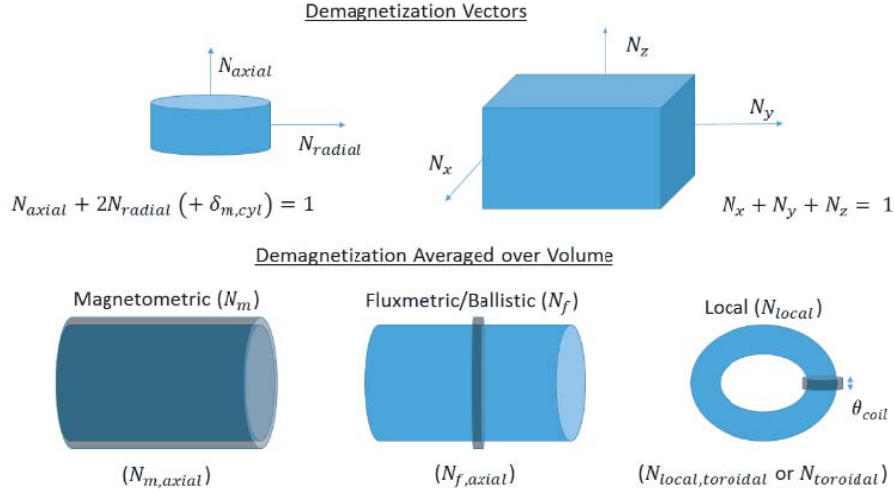
Figure 3. Demagnetization factors and geometry.
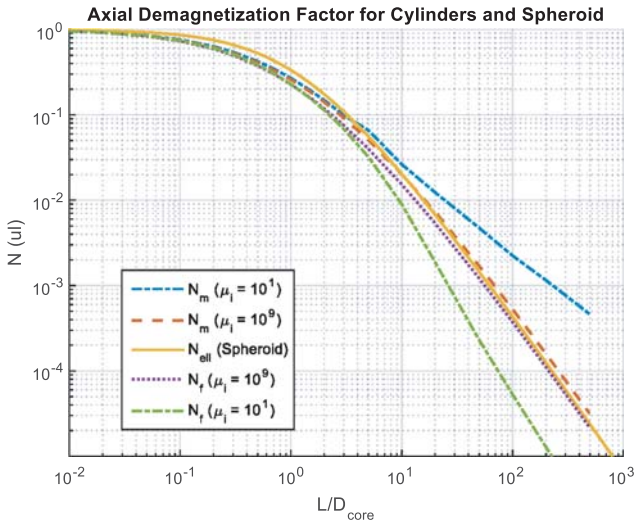
Figure 4. Axial demagnetization factors for solid cylinders and spheroid as a function of core length-to-diameter and initial permeability.

Figure 5. Axial, fluxmetric demagnetization factor for hollow and solid cylinders with infinite permeability as a function of core length-to-diameter and inner-to-outer diameter (ID/OD).

The common case of a coil centered axially on a solid, cylindrical magnetic core has been widely reported in literature. A reasonable, general approximation for the apparent fluxmetric permeability $\mu_{a,f}$ for such is [42]:

$$\mu_{a,f} \approx \frac{\mu_i \left[(l/d_{core})^{5/3} + 2.5 \right]}{\mu_i + \left[(l/d_{core})^{5/3} + 2.5 \right]}$$

where l/d_{core} is the length:diameter ratio of the core. Depending on the core dimensions, an asymptotic limit is reached such that further increases in initial permeability μ_i has greatly diminishing returns.

Besides solid cores, research has also been done on hollow cores [43–47]. The axial, fluxmetric demagnetization factor for hollow (and solid) cylinders of infinite permeability are presented in Figure 5. We observe that thick cores (inner: outer diameter ≤ 0.2) are essentially the same as solid cores and that

Rosenblat's formula [46] can be used to extend [47] for core length: diameter ratios greater than 0.8. Although infinite permeability is assumed, $\mu_i \gg 10$ appears sufficient [47]. For hollow cylinders with core length:diameter ratios greater than approximately 7 and very high μ_i, hollow prolate spheroidal equations are accurate.

Apparent permeability μ_a is then used to predict the effective permeability as a function of coil:core length and split it into the value for coil voltage (from an external magnetic field) as "external" permeability μ_{ext} and for coil inductance (and core resistance) as "internal" permeability μ_{int}. For solid cylinders with a centered coil, external permeability μ_{ext} can be accurately predicted with literature formulas, while internal permeability μ_{int} is more approximate. A comparison of measured and literature is presented in Figure 6 demonstrating the parabolic dependence on coil:core length for μ_{ext}. We recommend the following for predicting μ_{ext} & μ_{int} [1, 2]:

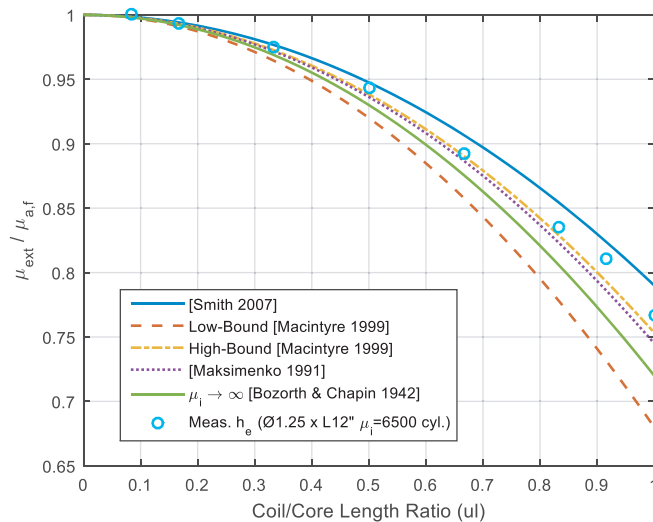$$\mu_{ext} \approx \mu_{a,f}\left[1 - k_{fm}\left(\frac{l_{coil}}{l_{core}}\right)^2\right]$$

$$k_{fm} = (1 - \mu_{a,m}/\mu_{a,f}) \approx 0.21\,[l/d_{core} \gg 1, \mu_i \gg 10]$$

$$\mu_{int} \approx \mu_{a,f}F; \quad F = \begin{cases} F_L & For\ L_{coil} \\ F_R & For\ R_{core} \end{cases}$$

$$F_L = -0.79\left(\frac{l_{coil}}{l_{core}}\right)^2 + 1.40\left(\frac{l_{coil}}{l_{core}}\right) + 0.09$$

$$F_R = -0.54\left(\frac{l_{coil}}{l_{core}}\right)^2 + 1.09\left(\frac{l_{coil}}{l_{core}}\right) + 0.01$$

where l_{core} is the core length.

Figure 6. Comparison of measured and literature formulas for solid magnetic-core cylinder effective external permeability (normalized by fluxmetric apparent permeability) versus coil-to-core length.

For hollow magnetic cores or for considering a coil that is not tightly wound onto a magnetic core, the effective permeability may be different than predicted. To a first-order, the effective permeability can be approximated by averaging the permeability over the volume. This results in the volumetric-averaged effective permeabilities $\mu_{vol,ext}$ and $\mu_{vol,int}$. While not necessarily accurate for internal permeability, measurements show that it can be for external. Note that some permeability and demagnetization references for hollow cores include correction for the internal hollow material's permeability, and some do not.

With the effective permeability known, an ESL's sensitivity (not to be confused with other sensitivity equations nor system sensitivity such as in [48]) can be calculated using the absolute

permeability of free-space μ_0, number of coil turns n, and coil area A_{coil}:

$$S_{min} = \mu_0 \mu_{vol,ext} n A_{coil} \left(\frac{V \cdot m \cdot s}{A} \right)$$

3. ESL DESIGN METHODOLOGY

Optimal design of an ESL requires consideration of multiple parameters including magnetic field sensitivity, bandwidth, impedance/noise matching to a preamplifier/receiver, volume, weight, target environment, and so on. For example, a space application requires lightweight, while a handheld device could be heavier but must be small. A dedicated fixed receiver could well be large and heavy. There may also be a target antenna impedance for optimal antenna matching and a minimum SRF.

Some general design tips and considerations are as follows. A short, centered coil on a magnetic core is optimal over a translated or full-length coil, and should be tightly wound onto the core. When winding a multi-layer coil, "fly-back" winding results in less self-capacitance C_{self} than "standard" winding, increasing the self-resonant frequency [35]. For multi-layer coils on a magnetic core, in order to minimize proximity effect losses, the optimum coil layout is trapezoidal (with the shorter length closest to the core) [14]. At low frequencies, expensive Litz wire has appreciable less resistive losses than solid or stranded wire. Aluminum wiring can be more effective than copper when weight is a consideration [49]. A hollow magnetic core's effective permeability can be almost as high as a solid core's but with a lot less weight. For a volume with large cross-section but short length, an air-core can be preferable.

It is not viable to *accurately* condense analytical theory, for example a sensitivity equation, except for very narrow applications. Instead, we suggest calculating the various parameters as per the following list and applying optimization weighting. It is important to check that all of the necessary assumptions are satisfied. Real, relative permeabilities are equal to one for air-core ESLs. The series resistance R and inductance L comprise several terms each due to internal wire impedance, external coil and mutual inductance, radiation resistance, core resistance, and impedance effects due to a surrounding medium or shield. The ordered list for calculating electrically-small loop antenna parameters is as follows:

1. Input physical and electromagnetic parameters.
2. Calculate apparent permeability μ_a.
3. Calculate external permeability μ_{ext} and internal permeability μ_{int}.
4. Calculate volumetric-averaged effective permeabilities $\mu_{vol,ext}$ and $\mu_{vol,int}$.
5. Calculate resistance R, inductance L, capacitance C, and sensitivity S_{min}.
6. Check assumptions.

Iterative evaluation of multiple designs can be done via a brute-force approach. For computationally-efficient approaches such as particle swarm optimization or backtracking search algorithms, consider the literature [50]. For a space application example, consider [51].

4. DESIGN EXAMPLE FOR AWESOME

In demonstrating our methodology, we design an optimal compact ESL for use with the AWESOME receiver which typically is paired with a large air-core loop. The main constraint of the AWESOME receiver is that its LNA is designed for antennas that are $1.0\,\Omega$ and between 0.5 and $1.0\,$mH impedance. The frequency range of interest was 1–100 kHz.

As the example is primarily illustrative, the sizes and materials were limited to those readily available by the authors: air-core (via wood or polyethylene) or ferrite-core (Ceramic Magnetics, Inc. MN60 Mn-Zn ferrite, $\mu_i = 6500$) that varied in length 3 to 12 inch (7.6 to 30.5 cm) and in core outer diameter (Ø) 1 to 1.75 inch (2.5 to 4.5 cm). Several of the considered ferrite core sizes were also evaluated for hollow. The coil lengths were varied from shortest-possible to full-length across the core, for 1/2/4 coil layers of 4–120 total coil turns, and for 4 types of wire (#24 stranded, #26 magnet wire, 60/36 Litz (60 strands of #36 magnet wire), and 120/36 Litz). Wire leads were 12 inches. Optimization weighting

was for maximum effective height (sensitivity) as long as the median impedance (across 0–100 kHz) was within specific bounds: $[0.8 < median\,(R_{ant}) < 1.2\,\Omega]$ & $[0.5 < median\,(L_{ant}) < 1.1\,\mathrm{mH}]$.

Since mass was not a concern, it is not surprising that the top two optimal designs were solid ferrite-cores that were the largest within the physical volume considered. The optimum coil lengths were short, which is common (although some literature recommends full-length coils; see [1] for more discussion and analysis). Along with an air-core triangular loop ("1") to compare against, the physical dimensions of these designs ("2" and "3") are given in Table 1 as-built. See Figure 7 for a photo of design 2.

Table 1. Loop physical descriptions.

|	1 — Air-Core	2 — Ø1.75-in Ferrite-Core	3 — Ø1.5-in Ferrite-Core
Core Length		12 in (30.5 cm)	12 in (30.5 cm)
Cross-Section	102 in (2.6 m) by 51 in (1.3 m) isos. triangle	Diameter 1.75 in (4.45 cm)	Diameter 1.5 in (3.81 cm)
Core Material	Air	MN60 Ferrite	MN60 Ferrite
Coil Length	0.5 in (1.3 cm)	2.5 in (6.35 cm)	2.44 in (6.20 cm)
Gross Weight	2 lb (0.9 kg)	5 lb (2.3 kg)	4 lb (1.7 kg)
# Turns	12	58	56

Figure 7. Photo of Ø1.75-in ferrite-core loop (design 2 in Table 1).

The two ferrite designs' measured and predicted series resistance R, inductance L, and sensitivity $S_{\min}$ (measured in a screen room by substitution method) are plotted in Figure 8–Figure 10, respectively. Predicted values for the air-core loop are also included. Error bars have been added for resistance and inductance; resistance is more difficult to measure accurately at higher frequencies as the reactive inductance dominates for these designs. Resistance can be accurately predicted at lower frequencies due to wire resistance dominating, while core losses dominate at higher frequencies and are more difficult to predict. Inductance is more difficult to predict for a magnetic core, with notable tolerances on the order of ±10–20% versus empirical data. Sensitivity prediction is very accurate. Overall, we find good agreement between measured and predicted.

Although the ferrite-core designs may be more optimal from a compact size perspective, they are less sensitive than the air-core they were compared against while they are similar in resistance and inductance. This is because sensitivity is proportional to effective permeability and coil turns-area product. Despite MN60 having a very high initial permeability of 6500, the effective external permeability is approximately 40 for these designs' dimensions while the air-core has a turns-area product that is 210–300 times larger. This means that a material of significantly less initial permeability could be used and/or the core hollowed out for little sensitivity loss.

To see how the designs worked in an *in situ* environment, the two ferrite designs were tested against the air-core with the AWESOME receiver by measuring the ambient electromagnetic spectrum in the natural environment. Measurements were taken during the daytime on April 7, 2016, at the Pisgah Astronomical Research Institute near Rosnay, NC (35.20N, 82.87W), an electromagnetically quiet site relatively free from interference from cities and power lines.

To conduct the measurements, the same receiver was used to take data from multiple loops simultaneously. Since the ferrite-core antennas have similar impedance as the air-core loop antenna, this gives an accurate comparison by ensuring that each loop is connected to an amplifier with the same noise figure. Furthermore, all three loops were oriented in the same direction. The data was calibrated for
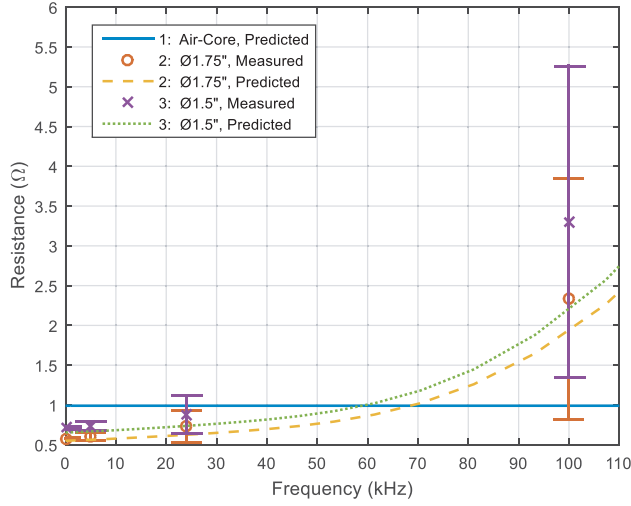
Figure 8. Measured and predicted series resistance of the loop antennas described in Table 1.
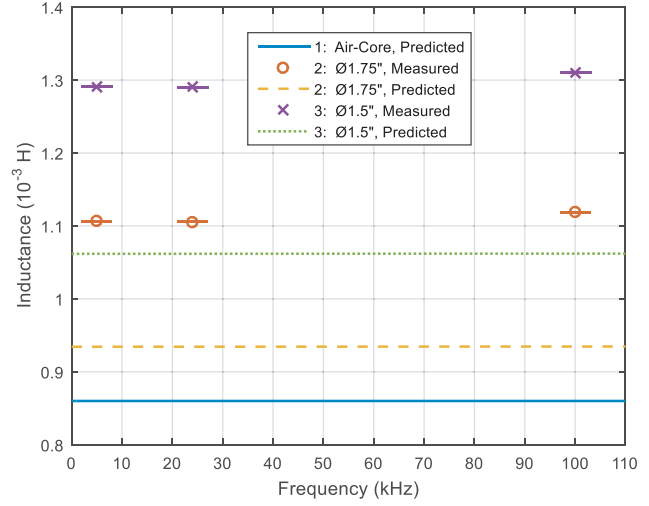
Figure 9. Measured and predicted series inductance of the loop antennas described in Table 1.
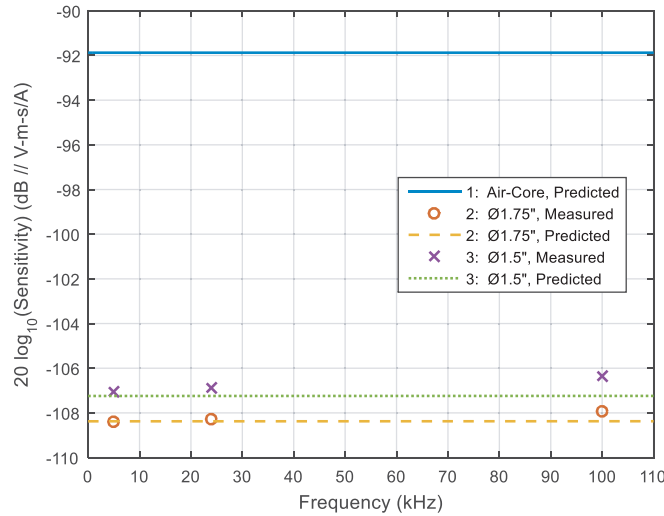

Figure 10. Measured and predicted sensitivity of the loop antennas described in Table 1.

the air-core loop antennas by injecting a known frequency-comb signal into the front end and digitizing the output, as described by [52]. The ferrite-core loops were not directly calibrated but can be using VLF transmitter signals, since this is a steady and constant signal during this period. Effectively, this means calibrating the ferrite-core loops by normalizing their gain difference with respect to the air-core loops.

A ten-second spectrum from 0–100 kilohertz (kHz) is shown in Figure 11. The spectrum peak at 24 kHz is the "NAA" United States transmitter at Cutler, Maine, at 800 kW; other VLF transmitters are visible from 19–41 kHz, especially for the air-core antenna. Peaks at the low end of the spectrum include power mains harmonics (60 Hz) and lightning sferics (from around the world).

For comparison, consider the antennas' spectrums around 24 kHz as shown in Figure 12. As expected, the air-core had the highest sensitivity, followed by the Ø1.75-inch ferrite-core then the Ø1.5-inch. At 24 kHz, the air-core is more sensitive by 11 and 13 decibels over the 1.75- and 1.5-inch ferrite-cores, respectively. As we discuss in [1], higher precision and accuracy in comparison could be undertaken but is not necessary for overall validation.
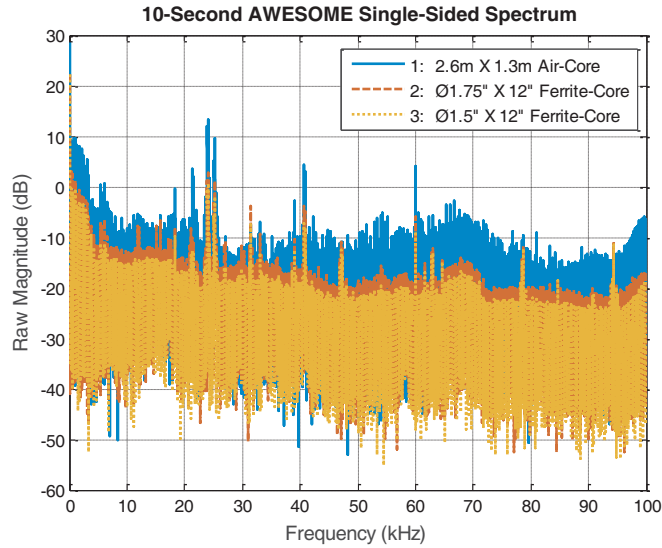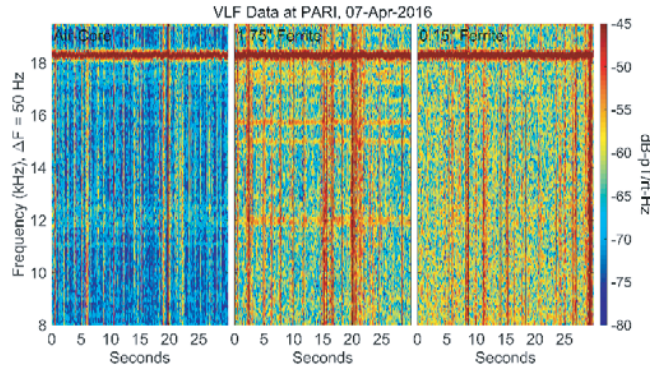
Figure 11. Measured ambient electromagnetic spectrum (10 seconds, single-sided) of the loop antennas described in Table 1 with the AWESOME receiver.
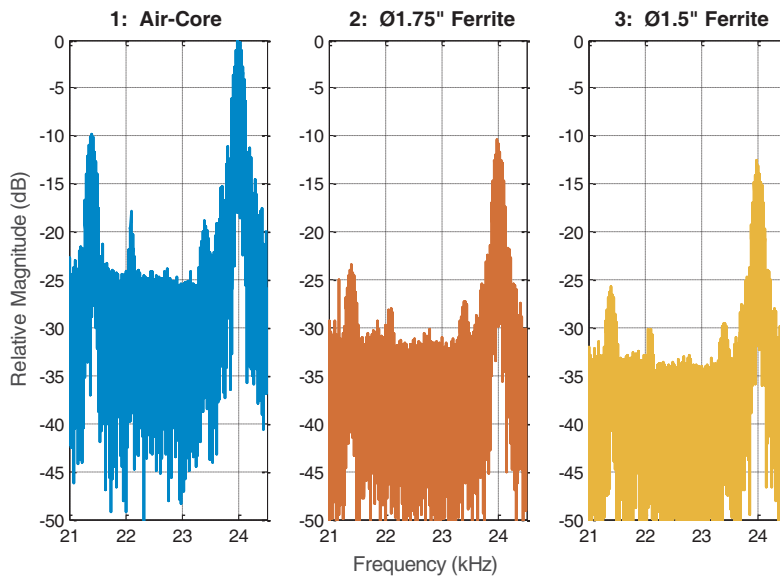
Figure 12. Narrowed spectrum of Figure 5 with magnitudes relative to the peak at 24 kHz.

Because of the impulsive nature of the background noise environment, dominated by VLF emissions from global lightning strokes, it is difficult for a single spectrum to capture the noise background inherent to a receiver during field measurements. Figure 13 shows another comparison in the form of a spectrogram, where each antenna has been normalized by its relative gain and calibrated. The spectrogram shows the Fourier transform in moving windows of time, after binning the data into 10 ms segments. This spectrogram is for a 30-second period, and shows a number of lightning-generated sferics as vertical lines representing impulsive signals, which typically dominate the VLF noise environment between 5–18 kHz. The horizontal line at 18.3 kHz is a VLF transmitter originating from France.

In reading this spectrogram, the most important feature to notice is the noise levels in between the impulsive sferics, which essentially represents the background noise intrinsic to the antenna. From this, it is clear that the air-core antenna has substantially better sensitivity by 10–15 dB compared to both

Figure 13. Measured ambient electromagnetic spectrogram (10 ms bins) of the loop antennas described in Table 1 with the AWESOME receiver.

of the ferrite-core antennas, despite being substantially lighter.

It should be emphasized that the 10–15 dB difference in the receiver noise levels in principle represents a lower bound, in that we can say that the ferrite-core antennas were limited by loop sensitivity and not by the environmental background, but we cannot be sure for the air-core loop. We also have laboratory calibrations of the air-core antenna which establish, for this size loop, a background noise level of -80–$85\,\mathrm{dB\text{-}pT}/\sqrt{\mathrm{Hz}}$, consistent with the background noise levels in the measured spectrogram for the air-core loop. Therefore, it seems likely that none of the receivers are actually limited strictly by environmental/atmospheric background, and the observations actually represent receiver noise levels.

When comparing the predicted sensitivities, the air-core loop is expected to be more sensitive than the Ø1.75-inch ferrite-core by 15 decibels (measured 11). The Ø1.75-inch measured approximately 2 decibels higher than the Ø1.5-inch in the field but 1.4 decibels in the laboratory. We believe that these differences are reasonable given the overall measurement uncertainty and conclude that the field testing validates the laboratory data.

We estimate that an air-core loop of Ø20-inch (0.5 m) with 19 coil turns would be equivalent to the Ø1.75-inch ferrite-core in terms of sensitivity. Therefore, the Ø1.75″ ferrite-core design achieves a reduced diameter at a cost of increased length and mass (the equivalent air-core is approximately 16 times less mass). Note that hollowing improves the mass/sensitivity ratio, as would using a different material with significantly less initial permeability (and less mass) as these ferrite cores were in the asymptotic limit for effective permeability for their μ_i and dimensions, but we have not considered those possibilities here.

In [52], it is shown that sensitivity of an air-core ESL antenna is proportional to $\sqrt{area \times mass}$ (with some assumptions). Normalizing the three designs' predicted sensitivity by this product, we calculate -93.4, -82.7, and $-81.2\,\mathrm{dB}/\!/\mathrm{V\text{-}s/A\text{-}kg}^{1/2}$ for the air-core, Ø1.75-, and Ø1.5-inch diameter ferrite loops, respectively. From this metric, the ferrite-core loops should be less sensitive than the air-core by slightly more than 10 dB, which is fairly consistent with the observed sensitivity difference in Figure 11 through Figure 13.

For additional background on measurements and design of electrically-small loop receiving antennas (including ferrite-core), the reader is directed to the literature such as [53–55].

5. CONCLUSION

We have presented a novel approach to optimal design of electrically-small loop receiving antennas based on electromagnetic design principles, demonstrated an application example at VLF/LF for two ferrite-core designs including optimal coil parameters (number of turns, layers, and placement on the core), and validated with experimental results. This design methodology allows an optimal design to be determined from a wide variety of inputs considering cost, size, and weight versus impedance and sensitivity in order to best fit the application need. In addition to laboratory measurements, we

have further validated our results with measurements of ambient signals with a sensitive, broadband AWESOME receiver.

Predicting the loop antenna impedance and sensitivity accurately is possible due to an extensive body of literature including empirical, analytical, and numerical investigations. We have included a description of the circuit model of an electrically-small loop antenna and recommended useful, accurate formulas for the predicted resistance, inductance, effective permeability, and sensitivity. Unfortunately, capacitance is more difficult to predict and it can be a limiting factor as it affects the self-resonant frequency. For magnetic core materials, the demagnetization factor and volumetric flux distribution results in an effective permeability (which affects resistance, inductance, and sensitivity) that is dependent on core geometry, material properties, and coil geometry upon the core. For most practical antennas, the effective permeability is a fraction of the core material's specified initial permeability resulting in significantly less sensitivity than at first glance. Our methodology is not limited by the core material, but we note that magnetic cores add uncertainty to predicting resistance and inductance. Further research is needed to more accurately predict capacitance as well as magnetic cores' resistance and inductance.

ACKNOWLEDGMENT

REFERENCES

1. Bolton, T. S., "Optimal design of electrically-small loop antenna including surrounding medium effects," M.S. thesis, Dept. Elect. and Comp. Eng., Georgia Inst. of Tech., Atlanta, GA, USA, 2016.

2. Smith, G. S., "Loop antennas," *Antenna Engineering Handbook*, 4th edition, Chap. 5, 5-1–5-25, J. L. Volakis (ed.), McGraw-Hill, 2007.

3. Snelling, E. C., *Soft Ferrites: Properties and Applications*, 390 Pages, Iliffe, 1969.

4. Balanis, C. A., *Antenna Theory: Analysis and Design*, 4th edition, Wiley, 2016.

5. Chen, D. X., E. Pardo, and A. Sanchez, "Fluxmetric and magnetometric demagnetizing factors for cylinders," *Journal of Magnetism and Magnetic Materials*, Vol. 306, 135–146, 2006.

6. Bozorth, R. M. and D. M. Chapin, "Demagnetizing factors of rods," *Journal of Applied Physics*, Vol. 13, 320–326, May 1942.

7. Cohen, M. B., U. S. Inan, and E. W. Paschal, "Sensitive broadband ELF/VLF radio reception with the AWESOME instrument," *IEEE Transactions on Geoscience and Remote Sensing*, Vol. 48, No. 1, 3–17, Jan. 2010.

8. Harriman, S. K., E. W. Paschal, and U. S. Inan, "Magnetic sensor design for femtotesla low-frequency signals," *IEEE Transactions on Geoscience and Remote Sensing*, Vol. 48, No. 1, 396–402, Jan. 2010.

9. Smith, G. S., "Proximity effect in systems of parallel conductors," *J. Appl. Phys.*, Vol. 43, No. 5, 2196–2203, May 1972.

10. Medhurst, R. G., "H.F. resistance and self-capacitance of single-layer solenoids," *Wireless Engineer*, 35–43, Feb. 1947; 80–92, Mar. 1947.

11. Dimitrakakis, G. S. and E. C. Tatakis, "High-frequency copper losses in magnetic components with layered windings," *IEEE Transactions on Magnetics*, Vol. 45, No. 8, 3187–3199, Aug. 2009.

12. Kazimierczuk, M. K., *High-Frequency Magnetic Components*, 2nd Edition, 756 Pages, Wiley Press, 2014.

13. Nan, X. and C. R. Sullivan, "An improved calculation of proximity-effect loss in high-frequency windings of round conductors," *Power Electronics Specialist Conference, 2003. PESC'03. 2003 IEEE 34th Annual*, Vol. 2, 853–860, 2003.

14. Spang, M. and M. Albach, "Optimized winding layout for minimized proximity losses in coils with rod cores," *IEEE Transactions on Magnetics*, Vol. 44, No. 7, 1815–1821, Jul. 2008.

15. Sullivan, C. R. and R. Y. Zhang, "Simplified design method for litz wire," *2014 IEEE Applied Power Electronics Conference and Exposition — APEC 2014*, 2667–2674, Fort Worth, TX, 2014.

16. Wojda, R. P. and M. K. Kazimierczuk, "Winding resistance of litz-wire and multi-strand inductors," *IET Power Electronics*, Vol. 5, No. 2, 257–268, Feb. 2012.

17. Tourkhani, F. and P. Viarouge, "Accurate analytical model of winding losses in round Litz wire windings," *IEEE Transactions on Magnetics*, Vol. 37, No. 1, 538–543, Jan. 2001.

18. Barrios, E. L., A. Ursúa, L. Marroyo, and P. Sanchis, "Analytical design methodology for litz-wired high-frequency power transformers," *IEEE Transactions on Industrial Electronics*, Vol. 62, No. 4, 2103–2113, Apr. 2015.

19. Sullivan, C. R., "Optimal choice for number of strands in a litz-wire transformer winding," *IEEE Transactions on Power Electronics*, Vol. 14, No. 2, 283–291, Mar. 1999.

20. Väisänen, V., J. Hiltunen, J. Nerg, and P. Silventoinen, "AC resistance calculation methods and practical design considerations when using litz wire," *Industrial Electronics Society, IECON 2013 — 39th Annual Conference of the IEEE*, 368–375, Vienna, 2013.

21. King, R. W. P. and G. S. Smith, *Antennas in Matter: Fundamentals, Theory and Applications*, 868 Pages, MIT Press, 1981.

22. Grover, F. W., *Inductance Calculations*, 304 Pages, Dover Publications, 2013, reprint of 1946 original.

23. Rosa, E. B. and F. W. Grover, "Formulas and tables for the calculation of mutual and self-inductance," *Bulletin of the Bureau of Standards*, Vol. 8, No. 1, 1916.

24. De Queiroz, A. C. M., "Mutual inductance and inductance calculations by Maxwell's method," Oct. 2014, http://www.coe.ufrj.br/~acmq/tesla/maxwell.pdf.

25. Snow, C., "Mutual inductance and force between two coaxial helical wires," *Journal of Research of the National Bureau of Standards*, Vol. 22, Research Paper RP1178, Feb. 1939.

26. Nagaoka, H., "The inductance coefficients of solenoids," *Journal of the College of Science (Imperial University, Tokyo, Japans)*, Vol. 27, No. 6, 1909.

27. Lundin, R., "A handbook formula for the inductance of a single-layer circular coil," *Proceedings of the IEEE*, Vol. 73, No. 9, 1428–1429, Sept. 1985.

28. Miller, H. C., "Inductance formula for a single-layer circular coil," *Proceedings of the IEEE*, Vol. 75, No. 2, 256–257, Feb. 1987.

29. Fincan, B. and Ö Üstün, "A study on comparing analytical methods for coil design in high frequency wireless energy transfer," *IEEE PELS Workshop on Emerging Technologies: Wireless Power (WoW), 2015*, 1–5, Daejeon, 2015.

30. Weaver, R., "Numerical methods for inductance calculation," accessed Mar. 2016, Parts 1–2 starting on http://electronbunker.ca/eb/CalcMethods.html.

31. Wheeler, H. A., "Simple inductance formulas for radio coils," *Proceedings of the Institute of Radio Engineers*, Vol. 16, No. 10, 1398–1400, Oct. 1928.

32. Simpson, T. L., "Effect of a conducting shield on the inductance of an air-core solenoid," *IEEE Transactions on Magnetics*, Vol. 35, No. 1, 508–515, Jan. 1999.

33. Young, J. C. and C. M. Butler, "Inductance of a shielded coil," *IEEE Transactions on Antennas and Propagation*, Vol. 49, No. 6, 944–953, Jun. 2001.

34. De Freitas Gutierres, L. F. and G. Cardoso, "Analytical technique for evaluating stray capacitances in multiconductor systems: Single-layer air-core inductors," *IEEE Transactions on Power Electronics*, Vol. 33, No. 7, 6147–6158, Jul. 2018.

35. Wu, B., X. Zhang, X. Liu, and C. He, "An analytical model for predicting the self-capacitance of multi-layer circular-section induction coils," *IEEE Transactions on Magnetics*, Vol. 54, No. 5, 1–7, Art No. 6201007, May 2018.

36. Ayachit, A. and M. K. Kazimierczuk, "Self-capacitance of single-layer inductors with separation between conductor turns," *IEEE Transactions on Electromagnetic Compatibility*, Vol. 59, No. 5,

1642–1645, Oct. 2017.

37. Knight, D. W., "The self-resonance and self-capacitance of solenoid coils: Applicable theory, models and calculation methods," Version 1.00, May 2016, DOI: 10.13140/RG.2.1.1472.0887, http://www.g3ynh.info/.

38. Mel'nikov, E. A. and L. N. Mel'nikova, "Receiving induction Ferrite antennas," *Izvestiya Vysshikh Uchebnykh Zavendeniy: Radioelektronika*, Vol. 17, No. 10, 1974.

39. Hole, M. J. and L. C. Appel, "Stray capacitance of a two-layer air-cored inductor," *IEE Proceedings — Circuits, Devices and Systems*, Vol. 152, No. 6, 565–572, Dec. 9, 2005.

40. Chen, D. X., J. A. Brug, and R. B. Goldfarb, "Demagnetizing factors for cylinders," *IEEE Transactions on Magnetics*, Vol. 27, No. 4, 3601–3619, Jul. 1991.

41. Chen, D.-X., E. Pardo, and A. Sanchez, "Demagnetizing factors of rectangular prisms and ellipsoids," *IEEE Transactions on Magnetics*, Vol. 38, No. 4, 1742–1752, Jul. 2002.

42. Poole, R. H. M., "Ferrite rod antennas for HF?" *R&D White Paper WHP 091 for British Broadcasting Corporation (BBC)*, Jul. 2004.

43. Wait, J. R., "The receiving loop with a hollow prolate spheroidal core," *Canadian Journal of Technology*, Vol. 31, 132–137, Jun. 1953.

44. Simpson, T., "Electrically small spheroidal loops wound on hollow Ferrite cores," *IEEE Antennas and Propagation Magazine*, Vol. 50, No. 3, 88–94, Jun. 2008.

45. Matyuk, V. F. and A. A. Osipov, "Central demagnetization factor for bodies with difference shapes. II. Rectangular rods," *Russian Journal of Nondestructive Testing*, Vol. 36, No. 1, 27–32, 2000.

46. Matyuk, V. F., A. A. Osipov, and A. V. Strelyukhin, "Central demagnetization coefficient for hollow cylindrical bars made of soft magnetic materials," *Russian Journal of Nondestructive Testing*, Vol. 43, No. 3, 154–162, 2007.

47. Kobayashi, M. and H. Iijima, "Surface magnetic charge distributions of cylindrical tubes," *IEEE Transactions on Magnetics*, Vol. 32, No. 1, 270–273, Jan. 1996.

48. Best, S. R., "Optimizing the receiving properties of electrically small HF antennas," *URSI Radio Science Bulletin*, Vol. 2016, No. 359, 13–29, Dec. 2016.

49. Burrows, M. L., "The submarine-towed ELF loop antenna," *Radio Science*, Vol. 11, No. 4, 357–366, Apr. 1976.

50. Duan, H. and Q. Luo, "Adaptive backtracking search algorithm for induction magnetometer optimization," *IEEE Transactions on Magnetics*, Vol. 50, No. 12, 1–6, Dec. 2014.

51. Coillot, C., J. Moutoussamy, P. Leroy, G. Chanteur, and A. Roux, "Improvements on the design of search coil magnetometers for space experiments," *Sensor Letters*, Vol. 5, No. 1, 1–4, 2007.

52. Paschal, E. W., *The Design of Broad-band VLF Receivers with Air-core Loop Antennas*, 2nd Edition, May 1988.

53. Rumsey, V. and W. Weeks, "Electrically small, ferrite-loaded loop antennas," *1958 IRE International Convention Record*, 165–170, New York, NY, USA, 1956.

54. Stewart, J., "On ferrite loop antenna measurements," *1958 IRE International Convention Record*, 42–48, New York, NY, USA, 1957.

55. Pettengill, R., H. Garland, and J. Meindl, "Receiving antenna design for miniature receivers," *IEEE Transactions on Antennas and Propagation*, Vol. 25, No. 4, 528–530, Jul. 1977.